JOURNAL OF MATERIALS SCIENCE 27 (1992) 5965–5981

Review
Use of spray techniques to synthesize particulate-reinforced metal-matrix composites

T. S. SRIVATSAN
Department of Mechanical Engineering, The University of Akron, Akron, OH 44325, USA
E. J. LAVERNIA
Materials Science and Engineering, Department of Mechanical and Aerospace Engineering, University of California, Irvine, CA 92717, USA

In an attempt to optimize the structure and properties of particulate-reinforced metal-matrix composites, a variety of novel synthesis techniques have evolved over the last few years. Among these, the technique of spray processing offers a unique opportunity to synergize the benefits associated with fine particulate technology, namely microstructural refinement and compositional modifications, coupled with *in situ* processing, and in some cases, near-net shape manufacturing. Spray technology has resurrected much interest during the last decade and there now exists a variety of spray-based methods. These include spray atomization and deposition processing, low-pressure plasma deposition, modified gas welding techniques and high velocity oxyfuel thermal spraying. Spray processing involves the mixing of reinforcements with the matrix material under non-equilibrium conditions. As a result, these processes offer an opportunity of modifying and enhancing the properties of existing alloy systems, and also developing novel alloy compositions. In principle, such an approach will inherently avoid the extreme thermal excursions, and the concomitant macrosegregation associated with conventional casting processes. Furthermore, the spray processing technique also eliminates the need to handle fine reactive particulates associated with powder metallurgical processes. In this paper, recent developments in the area of spray synthesis or processing of discontinuously reinforced metal-matrix composites are presented and discussed with particular emphasis on the synergism between processing, microstructure and mechanical properties.

1. Introduction

In recent years continuous attempts have been made, particularly in areas of alloy design and use of novel processing techniques, to develop high-performance hybrid materials or composites as serious competitors to traditional engineering alloys. In particular, much attention has been given to the development of reinforced metallic materials that offer significant improvements in structural efficiency, reliability and mechanical performance over the monolithic alloys. Interest in the use of metal-matrix composites for aerospace, automotive and other structural applications has gained increased importance as a result of an availability of relatively inexpensive reinforcements coupled with the concurrent development of various processing routes which result in reproducible microstructures and properties [1–3].

Reinforced metal matrices referred to as metal-matrix composites (MMCs) offer advantages in applications where low density, high strength and high stiffness are a primary concern. Early studies on MMCs addressed the development and behaviour of aligned, continuous fibre-reinforced materials based on aluminium and titanium matrices. Despite encouraging results, extensive industrial application of these composite materials has been hindered by competing aspects of exorbitant manufacturing costs and high labour-intensive manufacturing process coupled with their ability to offer highly directional properties such as high specific stiffness along the reinforcement direction [4]. Conversely, in applications where such extreme properties are not a requirement, the family of discontinuous metal-matrix composites consisting of particulates, whiskers, nodules and platelets, are preferred because they offer substantially improved strength and modulus properties compared to the monolithic alloy and provide an additional advantage of being machinable and workable. In particular, the particulate-reinforced metal-matrix composites are attractive because they exhibit near isotropic properties when compared to the continuously reinforced counterparts [5–13]. The primary disadvantage of all MMCs, however, is that often they suffer from low ductility, inadequate fracture toughness and inferior

0022–2461

fatigue crack growth performance compared to that of the constituent matrix material [14–19].

The discontinuously reinforced metal-matrix composites have attracted considerable attention on account of [5]:

(a) an availability of various types of reinforcements at competitive costs,

(b) the successful development of manufacturing processes to produce MMCs with reproducible structures and properties, and

(c) the availability of standard or near standard metal working methods such as casting, rolling, forging and extrusion which can be utilized to form these MMCs.

Furthermore, use of discontinuous reinforcements minimizes the problems associated with fabrication of continuously reinforced MMCs such as fibre damage, microstructural non-uniformity, fibre-to-fibre contact, and interfacial reactions. However, the discontinuously reinforced composite materials are not homogeneous and material properties are sensitive to properties of the constituent, interfacial properties and geometric shape of the reinforcement. Overall, the properties of particulate-reinforced metal matrices depend on:

(a) the size (diameter) of the reinforcing particle,

(b) the interparticle spacing,

(c) the volume fraction of reinforcement, and

(d) conditions at the matrix-reinforcement interface.

Also, needing to be considered are the matrix properties, including the work-hardening coefficient, which improves the effectiveness of the reinforcement constraint.

A thorough examination of the published scientific literature reveals that considerable research efforts have been expended on the development of a variety of novel processing techniques to optimize both the structure and properties of particulate-reinforced MMCs. Of the techniques developed and implemented, spray processing offers a unique opportunity to synergize the benefits associated with fine particulate technology, that is, refinements in intrinsic microstructural features, modifications in alloy chemistry, etc., coupled with *in situ* processing and, in some cases, near-net shape manufacturing. The technique of spray technology has evolved during the last decade, and there now exists a variety of spray-based methods. These include:

(a) spray atomization and deposition processing [20–32],

(b) low-pressure plasma deposition [33–37],

(c) modified gas welding technique [38], and

(d) high-velocity oxyfuel thermal spraying [39].

The technique of spray processing involves the mixing of discontinuous reinforcements with the matrix material under non-equilibrium conditions and, as a result, these processes offer:

(a) an opportunity of modifying and enhancing the properties of existing alloy systems, and

(b) development of novel alloy compositions.

It is the objective of this paper to present and discuss the recent and emerging developments in the area of synthesis of discontinuously reinforced metal-matrix composites using spray techniques. In particular, emphasis is placed on influence of the spray-processing technique on microstructure and mechanical behaviour. We begin with a discussion of the technique of spray atomization and deposition processing and follow it up with descriptions of the techniques of low-pressure plasma deposition, modified gas welding and high-velocity oxyfuel thermal spraying.

2. Spray atomization and deposition processing

During spray atomization and deposition, the unreinforced matrix material is disintegrated into a fine dispersion of droplets using high velocity inert gas jets. Simultaneously, one or more jets of the strengthening phase or phases, if more than one is required, are injected into the atomized spray at a previously determined spatial location. The spatial location is determined on the basis of numerical analysis of a fraction solid contained in the atomized matrix, as a function of the flight distance. This technique appears to offer some of the advantages of rapid solidification while at the same time minimizing the deleterious effects associated with oxidation. A comprehensive review of the technique, numerical analysis and results, and injection details are presented elsewhere [20, 21, 24, 40] and will not be reiterated here. The process is shown schematically in Fig. 1. In a recent study, Gupta *et al.* [20, 21] reported an optimum injection distance and substrate position to be 20 and 40 cm, respectively. Accordingly, at a flight distance of 20 cm, the atomized droplets have lost approximately 40% of their original enthalpy. Following co-injection, the mixture of rapidly quenched, partially solidified droplets with interdispersed ceramic particulates are deposited on a water-cooled deposition surface, eventually collecting as a coherent preform. The microstructure of the preform is governed by the solidification conditions during impact. To avoid extensive oxidation of the aluminium–lithium alloy during processing, the experiments were conducted inside an environmental chamber. The environmental chamber was evacuated down to a pressure of 4.0 μm mercury and backfilled with inert gas prior to melting and atomization. The primary objective of this technique is to achieve better and/or improved interfacial control by injection of the reinforcing particulates at a spatial location where a limited volume fraction of the atomized matrix spray is liquid. In this manner, a precise control of contact time, thermal exposure of the reinforcing particulates to the partially solidified matrix, and interfacial reactions is maintained.

2.1. Solidification and microstructure

Our current understanding of the distribution of reinforcing phases in the microstructure has improved with rapid advances in the field of reinforced materials. In a recent study, Gupta *et al.* [20, 21] incorporated up to 20 vol % silicon carbide particulates (SiC_p)

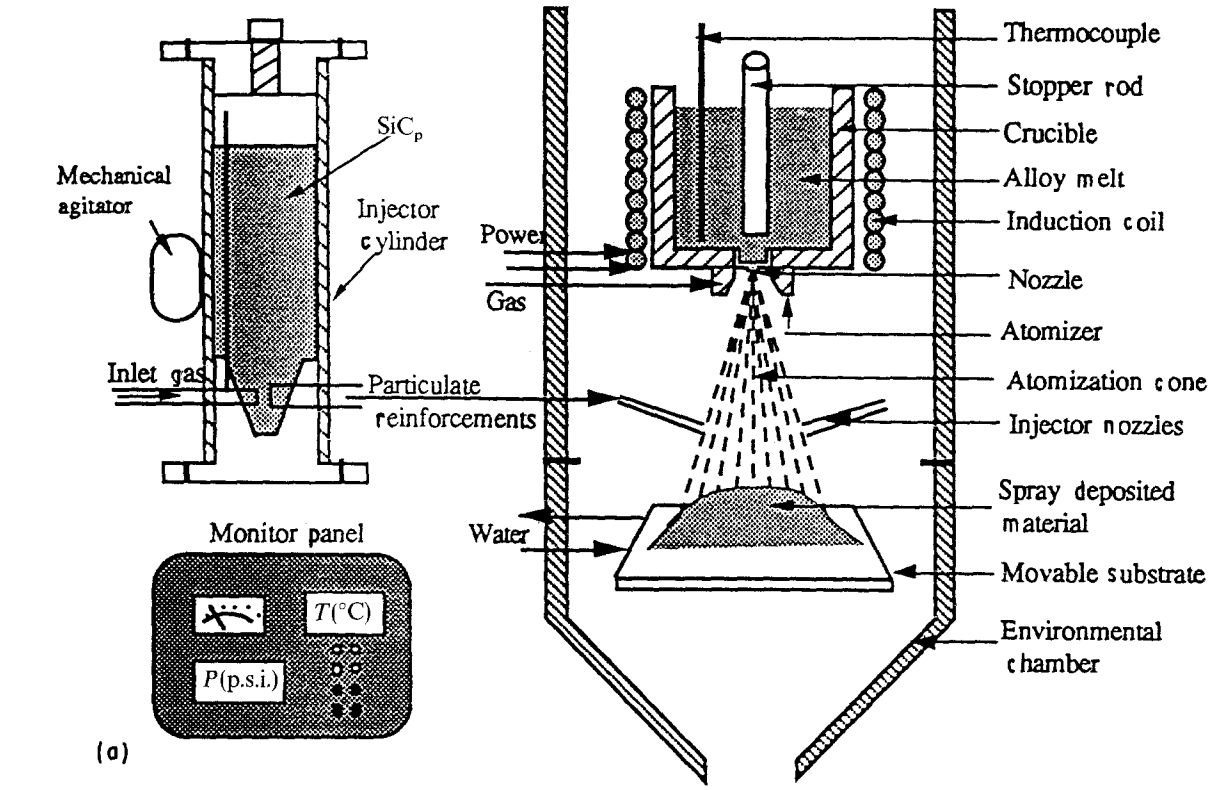

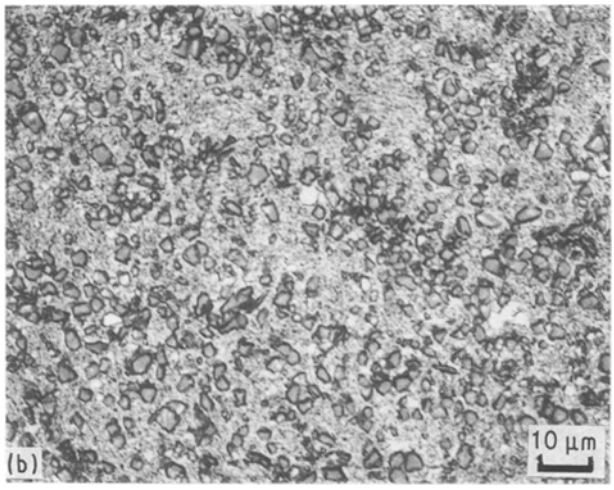

Figure 1 (a) Schematic drawing showing spray atomization and deposition processing of particulate-reinforced metal-matrix composites [24]. (b) Optical micrograph showing microstructure of spray-atomized and deposited 6061Al–SiC_p composite material containing 25 vol % particulates [49].

into the matrix of an aluminium–lithium alloy using spray atomization and deposition. In these experiments, injection of the reinforcing phase was accomplished by entraining SiC_p in an inert gas stream using a suitably designed fluidized bed. Table I, which is taken from the work of Gupta *et al.* [21], summarizes the results of an image analysis of the microstructure of five distinct experiments. The results shown in this table indicate that the angle of injection influences the distribution of SiC_p in the matrix, suggesting the possibility of tailoring any intrinsic variations in the volume fraction of the reinforcing phase through changes in injection angle. Regarding spatial variations in volume fraction of SiC_p, for a single experiment, the results shown in Table I do not provide a clear correlation between: (a) the spray-deposited thickness, (b) the amount of reinforcement (SiC_p), and (c) the experimental conditions. Although a systematic evaluation of the effects of injection angle on distribution of SiC_p was outside the scope of this particular study, the intrinsic variations in volume fraction of the discontinuous reinforcement with spray-deposited thickness, are most likely affected by changes in [21]:

(a) fluidization conditions, that is, pressure drop and particle velocity,

(b) the mass flow rate of the metal during the experiments, and

(c) the injection angle.

Furthermore, because the volume fraction of SiC_p was determined using image analysis, the results obtained should be treated as an order of magnitude approximation of the actual SiC_p volume fraction. The higher volume fraction of SiC_p observed in Experiment 2, was rationalized as being due to the existence of an "instant" pressurization condition at the metal delivery tube. This behaviour, which is caused by the relative position of the metal delivery tube to that of the gas jets, was exhaustively studied. The presence of a positive pressure at the tip of the metal delivery tube during atomization will tend to decrease the mass flow rate of the metal, thereby (a) effectively increasing the SiC_p/metal ratio, and (b) giving rise to abnormally high volume fractions of reinforcements. The results for the size distribution of silicon carbide particulates (SiC_p), from Table I, are consistent with the initial size of the SiC_p (d_{50} = 3.0 μm) used by Gupta *et al.* [21]. The slight reduction in particulate size was attributed to the difficulties associated with fluidizing the coarse reinforcing particles.

The resultant amount and distribution of reinforcing particles is of interest, because the mechanical

TABLE I Results of image analysis of Al–Li–SiC_p composite [20, 21]

Sample[a]	Equivalent diameter (μm)[b]				Volume fraction (%)				Interparticle spacing,
	Min.	Max.	Mean	σ	Min.	Max.	Mean	σ	λ (μm)
1A	0.57	09.00	2.70	2.01	1.92	08.33	3.49	1.82	14.48
1B	0.57	10.00	2.71	2.10	2.89	06.15	4.56	1.13	12.69
1C	0.57	12.00	2.10	1.76	4.40	13.44	7.89	1.91	07.48
2A	Not determined				–	–	9.60	–	08.71[d]
2C	Not determined				–	–	11.65[c]	–	07.91[d]
3A	0.57	11.00	2.76	2.13	4.69	7.19	6.12	0.85	11.14
3B	0.57	10.00	2.86	2.12	4.38	6.10	5.13	0.50	12.62
3C	0.57	9.00	3.34	2.16	1.34	3.16	2.49	0.54	21.16
4A	0.25	13.56	1.65	2.92	18.39	24.72	20.75	2.25	18.14
4B	0.25	9.33	1.54	2.34	3.17	07.36	05.41	1.56	25.71
5A	0.25	10.68	1.61	2.79	2.60	07.63	03.70	1.54	19.99
5B	0.25	16.95	2.27	4.24	2.77	08.95	06.00	2.29	11.89
5C	0.25	18.92	2.58	4.83	0.76	15.00	05.29	5.23	10.78

[a] A, B, C designations refer to top, centre and bottom regions, respectively, of the spray-deposited Al–Li–SiC_p.
[b] The equivalent diameter is a measure of the size of the SiC_p.
[c] These values of the volume fraction were determined using quantitative metallography.
[d] These values were computed for a SiC_p size of 2.7 μm.

behaviour of MMCs is dependent on both the amount and distribution of these particulates in the metal matrix. The distribution of reinforcing phases during processing of metal-matrix composites is of interest, because the mechanical behaviour of these materials is dependent on concurrent and competing influences of the size, distribution and orientation of these phases in the metal matrix. An interaction of the reinforcing phases, commonly ceramics, with solidification mechanisms governs the resultant distribution of the phase in the ductile matrix. A review of the published literature shows that over the last three decades several investigators have addressed the fundamental problem posed by the interaction of a particulate with a moving fluid front [41–48]. In particular, the results of these studies have enhanced our understanding of the kinetic and thermodynamic factors that govern the entrapment or rejection of particulates by a moving liquid front. According to the results made available from these studies, a particulate will be engulfed or rejected by a moving solidification front on the basis of one of the following criteria:

(a) thermodynamic criterion,
(b) critical velocity criterion,
(c) thermal conductivity criterion, and
(d) thermal diffusivity criterion.

These criteria were originally developed for steady state conditions, such as those present during equilibrium solidification (e.g. planar solid/liquid interfaces, spherical particles, and constant thermal properties). In contrast, the conditions present during spray atomization and deposition are far from being at equilibrium and, as previously discussed, involve both solid and liquid phases. However, in order to provide an insight into the kinetic mechanisms governing the distribution of silicon carbide particulates (SiC_p) during spray atomization and co-deposition, Gupta *et al.* [20, 21] used these criteria to predict engulfment or rejection of the particulates by the solidification front. The results of their study demonstrated that, whereas none of the four criteria predict particulate engulfment during solidification, the results of image analyses and microscopy (optical) studies indicated otherwise. For example, the results summarized in Table I indicate that the interparticle spacing for the SiC_p was in the 7–21.2 μm range, whereas the grain size was in the 66–72 μm range for all the experiments conducted. The results, which were supported by extensive optical microscopy and scanning electron microscopy observations suggest that SiC_p were located both intra- and intergranularly. The presence of SiC_p in the central region of the grains suggests engulfment of the particulates during solidification, because particulate rejection by the solidification front would result in pushing of the particulates towards the inter-dendritic regions.

The failure of the above criteria to account for the observed experimental results is not surprising in view of the extreme non-equilibrium conditions present during spray atomization and deposition. Therefore, because the microstructural characteristics of these materials could not be rationalized in terms of the aforementioned criteria, Gupta *et al.* [20, 21] explored the possibility of alternate mechanisms for particulate entrapment.

The volume fraction of SiC_p present in spray-atomized and co-deposited materials has been correlated with a number of processing parameters and physical properties such as [20, 21, 40, 49]:

(a) surface tension of the atomized droplets,
(b) injection angle,
(c) injection pressure, and
(d) SiC_p/metal mass flow rate.

The fine silicon carbide particulates are incorporated into the aluminium metal matrix by two possible mechanisms:

1. the SiC_p penetrate the atomized droplets during co-injection and remain entrapped in the matrix during subsequent impact with the deposition surface [40], and/or

2. the SiC_p remain on the surface of the atomized droplets and are entrapped by the matrix after impact with the deposition surface [49].

For the latter mechanism, it has been proposed that the extent of particulate entrapment after impact will depend on both the magnitude of the impact and the repulsive forces present at the metal/ceramic interface. This latter mechanism is discussed in detail by Gupta *et al.* [20, 21]. To rationalize the observed distribution of particulates in the metal matrix, a mechanism, termed mechanical entrapment, was proposed.

In the mechanically driven entrapment mechanism, a silicon carbide particulate is approached by multiple solidification fronts, as shown schematically in Fig. 2 [20, 21]. With convergence of the solidification fronts, a capillary region forms around the reinforcing particulates. At this point, the particulates will not only experience the repulsive forces from the adjacent solidification fronts but also capillary forces and fluid convective forces resulting from droplet impact and fracture. The combined effects of all three types of force will be to push the particulate(s) out of the capillary region. As the SiC particulate is displaced, subsequent impact by a droplet becomes highly probable as a result of the high spray density present during spray atomization and deposition. Because the impinging droplets arrive at the deposition surface

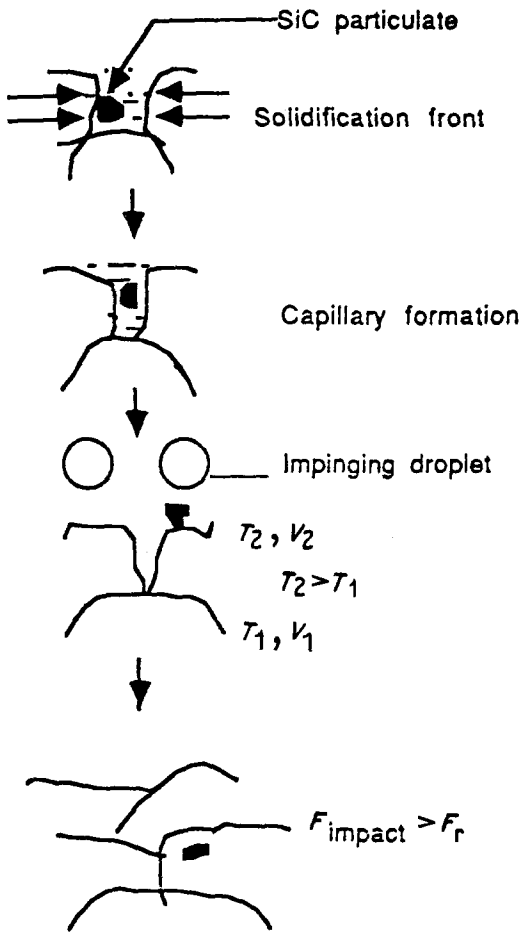

Figure 2 Schematic diagram showing mechanically driven entrapment during spray atomization and deposition processing: T_1, T_2, V_1 and V_2 refer to temperature and velocity before and after deposition [20, 21].

with velocities ranging from 100–400 m s^{-1}, depending on size, the high kinetic energy associated with the impact will lead to a mechanically stimulated engulfment of the ceramic particulates. This mechanism, however, assumes that the SiC particulates can move freely under the action of the aforementioned forces, and possesses a relatively smooth surface and a low aspect ratio.

Gupta *et al.* [20, 21] suggested the mechanical entrapment mechanism on the basis of a comparison of the magnitude of the repulsive forces acting on a particulate, as a result of the solidification front, F_r, to that of the impact forces exerted by the droplets, F_{impact}. Thus, when $F_{impact}/F_r > 1$ the particulate will be engulfed; otherwise it will be rejected. The repulsive forces experienced by a particulate due to effects of the solid/liquid front was computed from [20, 21]

$$F_r = \pi r \Delta\sigma_0/(n - 1) \quad (1)$$

where r is the radius of the particulate; $\Delta\sigma_0$ represents the difference in surface tension and n is a numerical constant. The impact force due to impinging droplets of size d_i was calculated from [39]

$$F_{impact} = V(d_i)\,\rho(d_i)\,a(d_i) \quad (2)$$

where $V(d_i)$, $\rho(d_i)$ and $a(d_i)$ represent the volume, density and acceleration of a droplet of size d_i, respectively. The value of the repulsive forces computed in accordance with Equation 1, and the impact forces computed in accordance with Equation 2 are summarized in Table II. In this table, d_{50} is defined as the mass mean droplet diameter of the aluminium matrix, that is, the opening of a screening mesh which permits through 50% of the mass of the powder resulting from an atomization experiment. It can be seen from the results summarized in Table II, that the impact forces resulting from the d_{16} droplets are not sufficient to overcome the repulsive forces for a large proportion of the SiC particulate sizes used in this study. However, the impact force exerted by the d_{50} and d_{84} droplets can lead to an engulfment of the 1, 3 and 5 μm particulates. Because the d_{50} and d_{84} droplets comprise of a large proportion of the entire distribution, it is concluded that a large proportion of the silicon carbide particulates should be engulfed. These predictions were found to be consistent with the experimental findings [20, 21].

If entrapment fails to take place either during co-injection, or subsequently, during deposition, the microstructure of the spray-atomized and co-deposited materials will be characterized by a high concentration of ceramic particulates at the prior particle boundaries. Ibrahim *et al.* [49] reported such a situation to exist for the spray-atomized and co-deposited 6061/SiC_p composite.

2.2. Room-temperature behaviour of aluminium composites

Several studies have been conducted, in recent years, to understand the room-temperature mechanical behaviour of spray-atomized and deposited metal-matrix composites [26, 38, 51–53]. Ibrahim *et al.* [49],

TABLE II Computed repulsive and impact forces during deposition [20, 21]

Repulsive force (N)	Impact force[a] (N)	Prediction
$F_r(1\ \mu m) = 4.33 \times 10^{-6}$	$F(d_{16}) = 2.51 \times 10^{-6}$	Engulfment not possible for 1, 3 or 5 μm particulate size
$F_r(3\ \mu m) = 1.30 \times 10^{-5}$	$F(d_{50}) = 3.00 \times 10^{-5}$	Engulfment possible for 1, 3 and 5 μm particulate size
$F_r(5\ \mu m) = 2.16 \times 10^{-5}$	$F(d_{84}) = 3.14 \times 10^{-4}$	Engulfment possible for 1, 3 and 5 μm particulate size

[a] d_{16} (30.4 μm), d_{50} (86.0 μm) and d_{84} (243.2 μm) characterize the droplet size distribution.

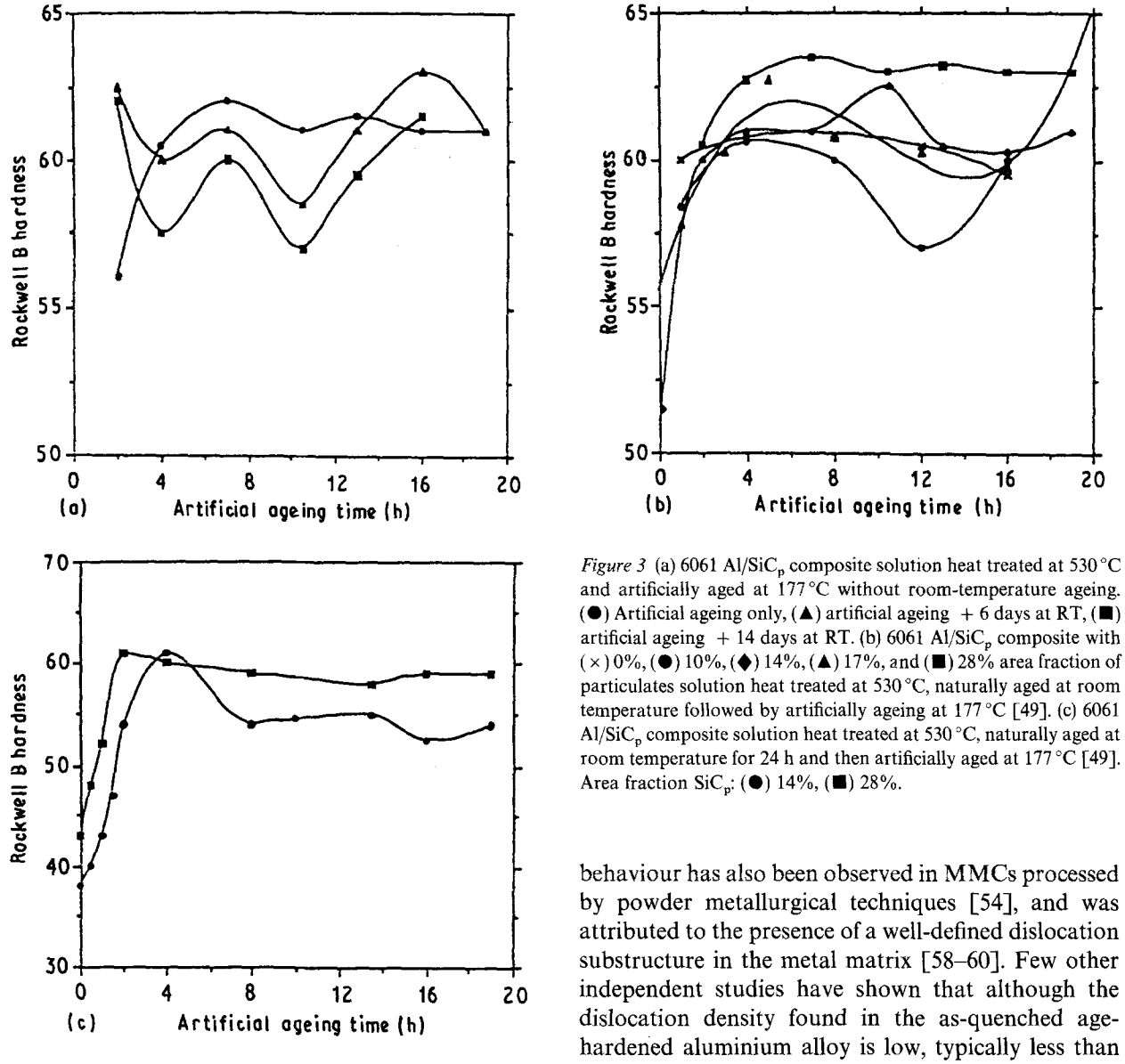

Figure 3 (a) 6061 Al/SiC_p composite solution heat treated at 530 °C and artificially aged at 177 °C without room-temperature ageing. (●) Artificial ageing only, (▲) artificial ageing + 6 days at RT, (■) artificial ageing + 14 days at RT. (b) 6061 Al/SiC_p composite with (×) 0%, (●) 10%, (◆) 14%, (▲) 17%, and (■) 28% area fraction of particulates solution heat treated at 530 °C, naturally aged at room temperature followed by artificially ageing at 177 °C [49]. (c) 6061 Al/SiC_p composite solution heat treated at 530 °C, naturally aged at room temperature for 24 h and then artificially aged at 177 °C [49]. Area fraction SiC_p: (●) 14%, (■) 28%.

studied the microstructure and mechanical properties of spray-atomized and deposited 6061Al/SiC_p materials, reinforced with 3 and 15 μm size particulates. The results of their study showed that the presence of SiC_p alters the ageing response of the spray-atomized and deposited materials, relative to that observed for the unreinforced alloys. The results of the ageing studies, for increasing amounts of SiC_p reinforcement, are summarized in Fig. 3. The results shown in this figure, which are consistent with those reported by other investigators [54–58], suggest that the ageing time required to attain maximum hardness was significantly reduced in the reinforced material when compared to that of the unreinforced matrix alloy. This behaviour has also been observed in MMCs processed by powder metallurgical techniques [54], and was attributed to the presence of a well-defined dislocation substructure in the metal matrix [58–60]. Few other independent studies have shown that although the dislocation density found in the as-quenched age-hardened aluminium alloy is low, typically less than $10^5\ cm^{-1}$ [59], the dislocation density in reinforced aluminium metal matrices is of the order of $10^{13}\ cm^{-1}$ [60]. These dislocations, which are generated in order to accommodate the thermal mismatch strains associated with differences in the thermal coefficient of expansion (CTE) of the metal matrix and the reinforcement, are located primarily at the reinforcement–matrix interface, and decrease with an increasing distance from the interface [60]. As the nucleation site density is proportional to the dislocation density, an increase in nucleation rate is to be anticipated for reinforced metal matrices. Furthermore, the results shown in Fig. 3 reveal that natural ageing tends to accelerate the subsequent artificial ageing response of the reinforced aluminium alloy 6061 (Figs 3a and c). A

similar observation has been documented elsewhere [57].

Following spray atomization and deposition, Ibrahim *et al.* [49] studied the room-temperature mechanical behaviour of hot-extruded materials; the results of which are summarized in Table III. The influence of area fraction of reinforcing SiC_p on mechanical behaviour can be seen from this table. The results suggest an improvement in tensile strength with a concomitant degradation in tensile elongation with an increase in area fraction of the reinforcing SiC_p phase. This finding is consistent with an increase in dislocation density, with a simultaneous enhancement in dislocation–particle interactions, accompanying an increase in volume fraction of particulates in the metal matrix. Also evident from the results shown in Table III is the significant effect of thermal treatment on the tensile behaviour of metal-matrix composites. The decrease in ultimate tensile strength and tensile yield strength of the spray-deposited and extruded materials, relative to that of a PM alloy 6061 MMC was attributed to the synergistic influences of the presence of a fine dispersion of oxide phases in conjunction with a higher volume fraction of particulates in the matrix of the PM material.

In other studies, White *et al.* [63] examined the structure and properties of a spray-cast Al–Li–Cu–Mg–Zr alloy (8090) reinforced with SiC and B_4C particulates. The mechanical properties of the spray-cast and hot-extruded materials are summarized in Table IV, and compared to those of equivalent ingot alloys. The results showed that the most significant property improvement was the elastic modulus. The elastic modulus of the spray-cast material was 25% higher than that of the corresponding ingot counterpart. Further improvements in mechanical behaviour of spray-cast materials were achieved by introducing cold deformation prior to artificial ageing [63].

Srivatsan *et al.* [52, 64] evaluated the cyclic fatigue, stress response and cyclic fracture characteristics of the aluminium alloy A356 (7% Si, 0.2% Cu, 0.35% Mg, 0.1% Mn, 0.2% Fe, 0.1% Zn and balance aluminium) reinforced with 20 vol % silicon carbide particulates and processed by spray atomization and deposition technique. They also compared the cyclic strain resistance of the processed metal-matrix composite material [A356/SiC_p] with the as-cast counterpart also containing 20 vol % of reinforcement (SiC_p). The microstructure of the spray-atomized and deposited metal-matrix composite material (referred to as the processed microstructure) revealed the reinforcing silicon carbide (SiC) particulates to be of near uniform size and dispersed uniformly in the aluminium alloy matrix (Fig. 4). The microstructure also revealed no evidence of an agglomeration of SiC particulates. The cyclic stress response curves or cumulative glide plots of stress amplitude during a low-cycle fatigue (LCF) test versus number of cycles, at fixed plastic strain amplitudes, are shown in Fig. 5. At lower cyclic strain amplitudes, the stress response of the composite showed a period of cyclic stability culminating in rapid softening prior to failure, due to the onset of macrocrack initiation and growth. It was also observed that the spray-atomized and deposited material

TABLE III Room-temperature mechanical properties of spray-atomized and extruded materials [49]

Material	Temper	Area fraction	σ_{UTS} (MPa)	σ_{YS} (MPa)	Elong. (%)
IM 6061	T6	0	290	255	17.0
Unreinforced	T4	0	187	96	29.0
Unreinforced	T6	0	345	301	10.0
β-SiC_p	T4	10	207	96	25.0
β-SiC_p	T6	10	285	262	14.0
α-SiC_p	T4	14	196	104	23.0
α-SiC_p	T6	14	330	294	9.0
α-SiC_p	T6	17	337	299	7.0
α-SiC_p	T4	28[a]	252	147	12.0
α-SiC_p	T6	28[a]	362	322	5.0
PM 6061 [61]	T6	40	540	486	0.6
PM 6061 [62]	T6	20	498	415	6.0

[a] The SiC particulate size used here was 15 μm; all other tests were conducted with 3 μm particulates.

TABLE IV Room-temperature mechanical properties of spray-atomized and extruded 8090 [26]

Material	Volume fraction	σ_{UTS} (MPa)	σ_{YS} (MPa)	Elong. (%)	E (MPa)
8090	–	520	480	5.0	79.5
8090	12[a]	529	486	2.6	100.1
8090	11[b]	445	410	1.6	98.1

[a] SiC particulate size used here was 13 μm.
[b] B_4C particulate size used here was 13 μm.

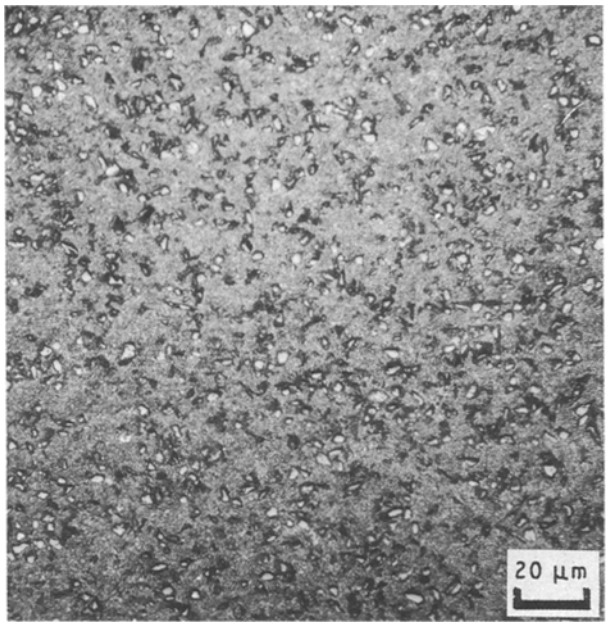

Figure 4 Optical micrograph showing microstructure of the spray-atomized and deposited A356 + 20 vol % SiC_p composite [52].

withstood considerably higher cyclic strain amplitude and concomitant response stress (Fig. 5a) than the as-cast counterpart (Fig. 5b). The difference in cyclic stress response characteristics between the as-cast and the spray-processed microstructures of A356 + 20 vol % SiC_p composite was rationalized by Srivatsan *et al.* [52, 53] as being due to processing influences on composite microstructure resulting in a change in particle size, morphology and distribution with a resultant change in dislocation–SiC_p interaction, and thus, microcrack initiation and growth. The interaction of mobile dislocations with the SiC particles dominates during the initial stage of cyclic deformation. When the local stress concentration caused by dislocation build-up at a silicon carbide particulate (SiC_p) exceeds a critical value, microcrack initiation occurred through rupture of the hard and brittle particle. With continued cyclic deformation, numerous such particles crack on account of their intrinsic brittleness. The microcracks, initiated at neighbouring particles, rapidly link to form a macroscopic crack resulting in a drop in load-carrying capability or softening of the composite material prior to failure.

The effect of strain cycling on LCF life of the A356 + 20 vol % SiC_p composite is shown in Fig. 6. This curve can be viewed as an indication of the resistance of the material's microstructure to crack initiation and failure. The plastic strain–fatigue life curve was found to be linear and the Coffin–Manson relationship [65, 66] could be used to determine or predict fatigue behaviour in the LCF regime ($N_f < 10^4$ cycles). The values of fatigue ductility exponent, C, and fatigue ductility coefficient, ε_f' (= 3.02% for as-cast composite and 9.5% for spray-atomized and deposited composite) indicated the spray-processed microstructure to have better cyclic strain resistance and cyclic ductility than the as-cast composite microstructure, with a resultant 300% to 400% improvement in low-cycle fatigue life or cyclic strain resistance [52, 53].

Cyclic fracture of the spray-processed A356/SiC_p composite, on a macroscopic scale, revealed ductile failure with isolated microcracks in the matrix (Fig. 7a). High-magnification observation revealed large areas of the fracture surface to be covered with a bimodal distribution of dimples (Fig. 7b) indicative of ductile rupture. The fracture behaviour of the spray-atomized and deposited composite accorded well with the improved cyclic stress and cyclic strain resistance [52, 53].

3. Low-pressure plasma deposition

Synergizing the two independent operations of powder synthesis and their consolidation, involved in rapid solidification processing, into a single step or operation led to the emergence of the technique of spray-deposition processing. This attractive technology, facilitated an achievement of metallurgical and chemical homogeneity, was used for the direct fabrication of a whole variety of simple preform shapes, such as tubes, discs, ingots, etc. Around the same time, a new process was developed by the General Electric Company for net shape processing by plasma spraying in a reduced pressure environment. This technique was called low-pressure plasma deposition (LPPD). Unlike the technique of spray deposition, the unique feature of the LPPD process is that it makes use of prealloyed powders as the feedstock coupled with an intrinsic difference in the manner in which the sprayed deposit is built-up into the monolithic shape.

The low-pressure plasma spray-deposition technique combines particle melting, quenching and consolidation in a single operation. The process involves an injection of a variety of powder particles ranging from metallic to ceramic, and including mixtures, into a plasma jet stream created by heating an inert gas in an electric arc confined within a water-cooled nozzle. The particles injected into the plasma jet, at temperatures of 10 000 K and higher, undergo rapid melting and are accelerated towards the workpiece surface. Rapid quenching of the molten particles occurs when the droplets impact the substrate. Cooling rates are very high, of the order of 10^5–10^6 K s^{-1}, and the resulting microstructure is fine-grained and homogeneous.

The technique of conventional plasma spraying (CPS) is normally carried out at atmospheric pressure. The resultant deposit contains oxidation products, together with some porosity due to incomplete melting, wetting or fusing together of deposited particles. The problem of oxidation is overcome or minimized either by shielding the plasma arc with an inert gas atmosphere, or by enclosing the entire plasma-spraying unit in an evacuated chamber, which is maintained at about 30–60 torr (1 torr = 133.322 Pa) inert gas pressure by high-speed pumping. Under the latter operating conditions of low-pressure plasma deposition (LPPD), gas velocities are high (typically in the Mach 2–3 range) due to the higher permissible pressure ratios. When the inert gas or environment is vacuum, the technique is referred to as vacuum plasma spraying (VPS) [34–37]. Other noteworthy

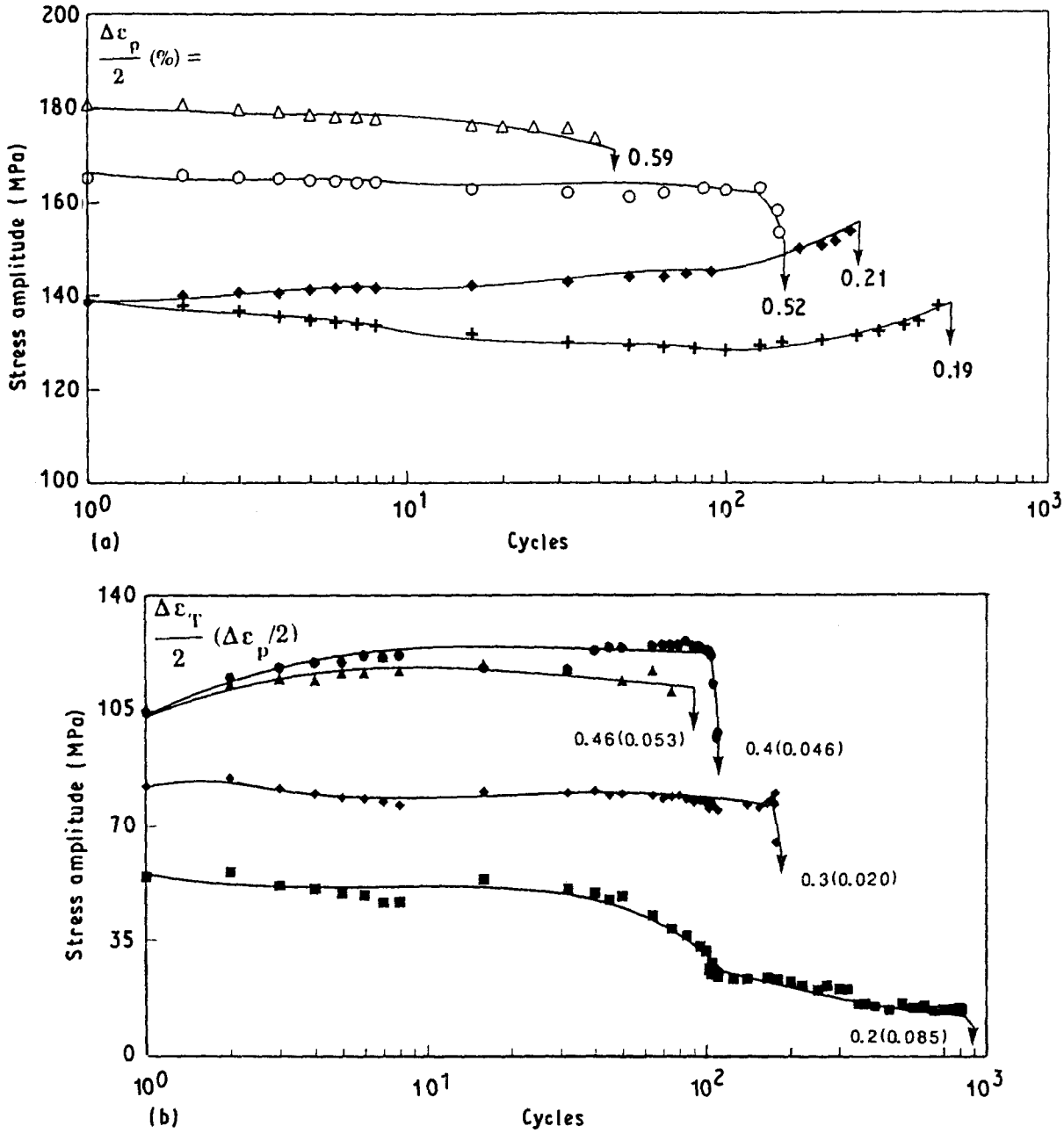

Figure 5 (a) Cyclic stress response curves for the spray-atomized and deposited A356 + 20 vol % SiC_p composite material [52, 53]. (b) Cyclic stress response curves for the as-cast A356 + 20 vol % SiC_p composite material [52, 53].

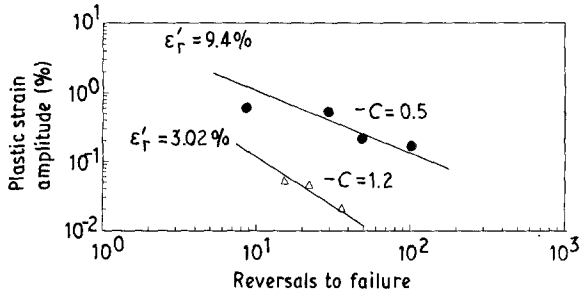

Figure 6 Comparison of the influence of microstructure on plastic strain–fatigue life response of the A356 + 20 vol % SiC_p composite: (△) as-cast, (●) processed [52, 53].

advantages of LPPD and VPS, compared with CPS, include [33, 34, 67]:

(a) higher particle velocities, which give rise to denser deposits (often > 98% theoretical density),

(b) broad spray patterns, which produce large areas of relatively uniform deposition characteristics, and

(c) automatic regulation of the technique to produce controlled deposits of complex geometries at reasonably high deposition rates (up to 50 kg h^{-1}).

The four basic components of a typical plasma gun, namely (1) cathode, (2) arc chamber, (3) throat, and (4) exit nozzle, are shown in Fig. 8. The cathode and anode are located concentrically and are water cooled to prevent melting by the high gas temperatures. An arc gas (argon or mixture of argon and helium) is fed from behind the cathode. The arc gas is fed tangentially, creating a vortex that acts to stabilize the electric arc. Powder injection ports are located within the nozzle (anode), or downstream of the nozzle, depending primarily on:

(a) the characteristics of the plasma gun, and

(b) the type of powder being sprayed.

Protection against environmental interactions, after particle melting has resulted, is achieved by injecting a shroud of inert gas around the periphery of the jet

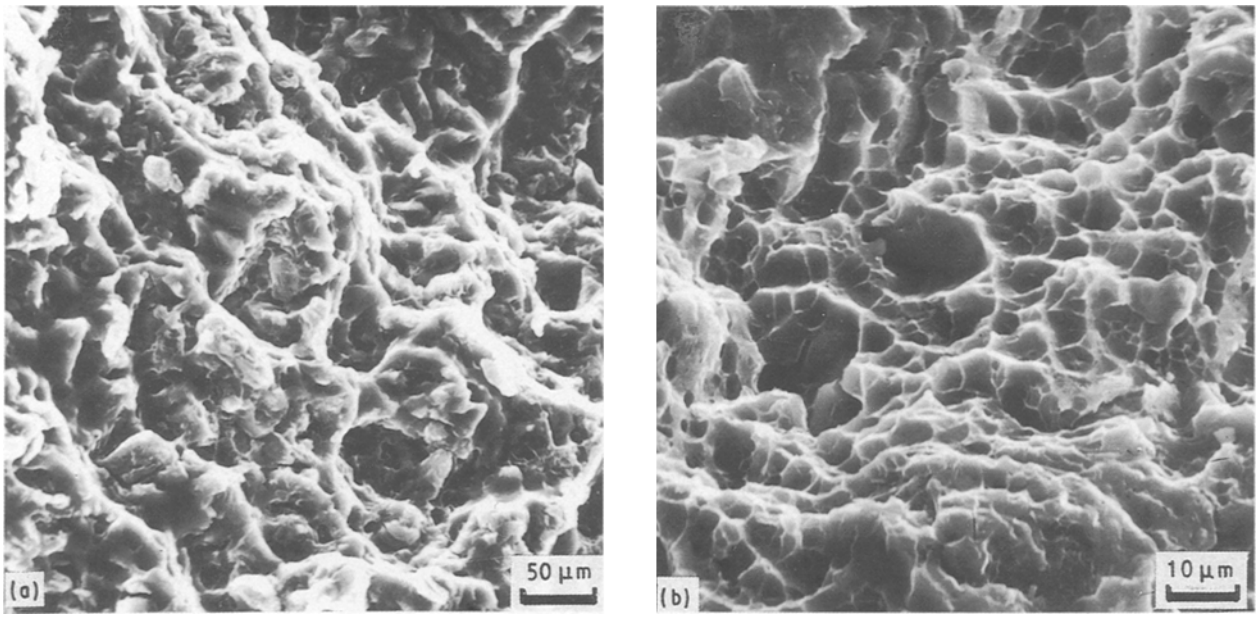

Figure 7 Scanning electron micrographs showing fracture surface features of the spray-atomized and deposited composite: (a) isolated microcracks in the matrix; (b) ductile dimples [52].

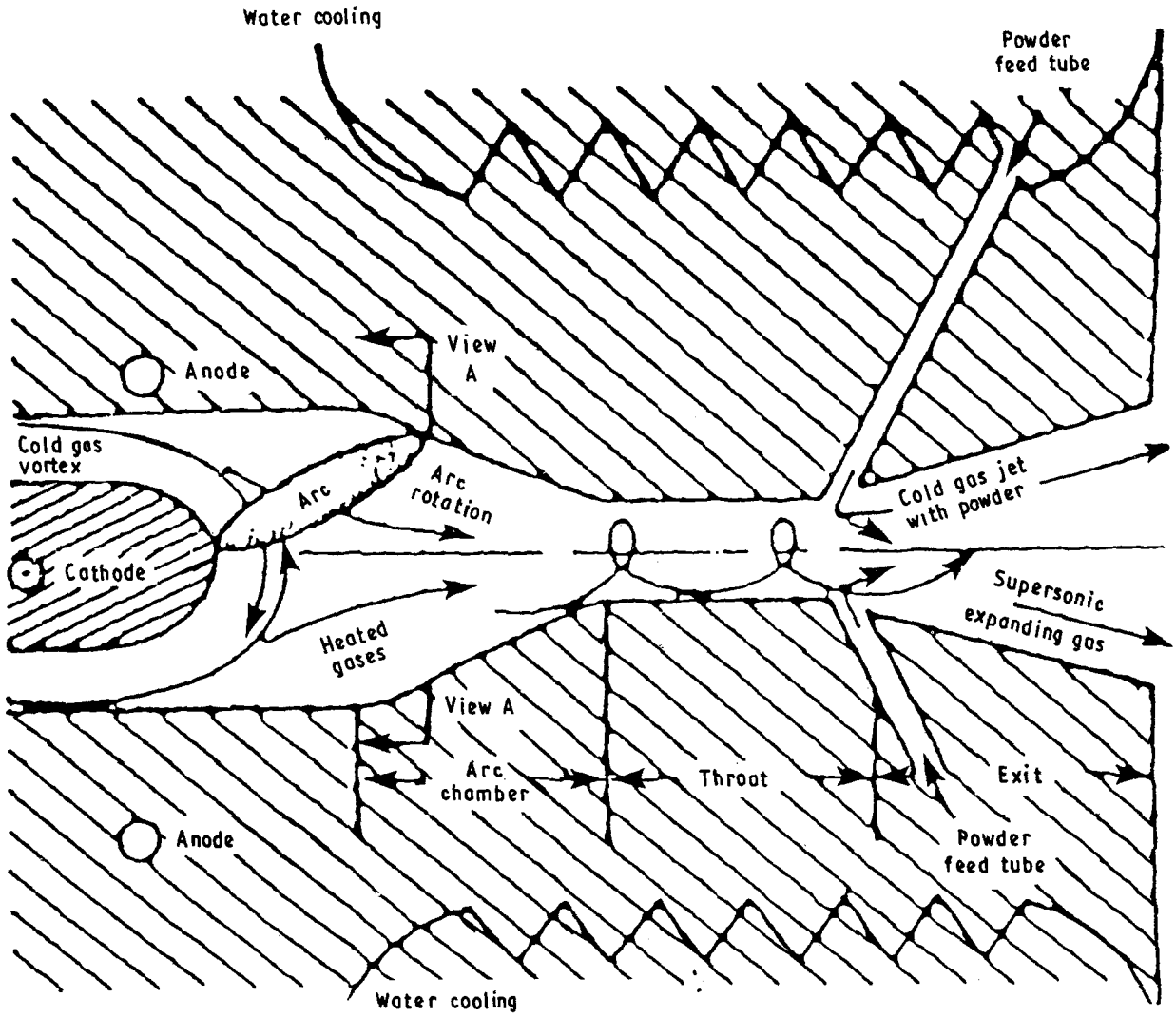

Figure 8 Cross-sectional schematic drawing of the plasma-gun showing the supersonic expanding gas jet [38].

and/or around the substrate. The reduced inert gas pressure environment ensures that the particles/droplets are protected from oxidation. By minimizing environmental interactions, high-quality metallurgically sound deposits, which are well bonded to the substrate, are achieved by the LPPD technique.

The fine metal particles are injected into the plasma flame, where they are melted and accelerated to high

velocities (200–300 m s^{-1}) towards the substrate. The particles impact the substrate and rapidly solidify. A rapid solidification rate (RSR) deposit is build-up by the successive impingement of molten particles. During the course of deposition processing, the substrate–deposit system is exposed to temperatures of 800–900 °C, due to an interaction with the hot plasma flame and the heat of solidification. The resultant annealing, due to the high-temperature exposure, was found to be beneficial, because it: (a) provided stress relief to the deposit, (b) improved interparticle bonding, and (c) promoted recrystallization to occur without appreciable grain growth, thereby essentially retaining the characteristics of rapid solidification rate (RSR) processing [36].

The resultant deposits, of the LPPD process, typically have fine microstructures, and contain varying amounts of retained porosity and inclusions, depending on deposition parameters, such as power level, arc gas composition, jet transport properties and the level of reduced pressure. The protected atmosphere minimizes the number of oxide-containing inclusions and the density of pores. The resultant deposit contains fewer inclusions and the density achieved under conditions of low-pressure plasma spraying is about 98% theoretical density.

The use of the low-pressure plasma deposition or VPS technique for superalloys resulted in significant improvement in strength. This was attributed to synergistic and competing influences of microstructural (grain size) refinement, microstructural homogeneity, and extended solubility of solid solution strengtheners. While the tensile strengths of the LPPD superalloys were comparable with the wrought counterparts, over the entire range of interest, the ductilities of the LPPD product were found to be inferior to the wrought product in the high-temperature range, above 1400 °C (Fig. 9). The improvement in ductility was attributed to recrystallization of the wrought product [33]. Appreciable improvement of thermal fatigue performance was also observed for LPPD superalloys compared to the as-cast material. The emergence of the LPPD technology lead to an availability of quality coatings of high-performance materials. The coatings found application in industrial gas turbines and jet engines. Furthermore, an ability to control the deposition of the material at high temperatures coupled with sound metallurgical quality facilitated use of the LPPD technology to build up thick (> 5 cm) deposits without sacrificing quality.

Few studies have been performed on low-pressure inert gas atmosphere sprayed intermetallics [34]. In comparison with other RSR approaches (e.g. splat quenching and melt spinning), this technique offered the advantages of large throughputs (kg h^{-1}), high density, an ability to coat objects of complex shape, and the production of near-net shape bulk forms. Chang *et al.* [69] compared the mechanical properties of melt-spun ribbons, hot isostatically pressed specimens and plasma-spray consolidated $Ni_3Al + B$ alloys. They found the plasma-sprayed specimens to have the highest yield and ultimate tensile strengths, with adequate ductility. The fine-grained structure of

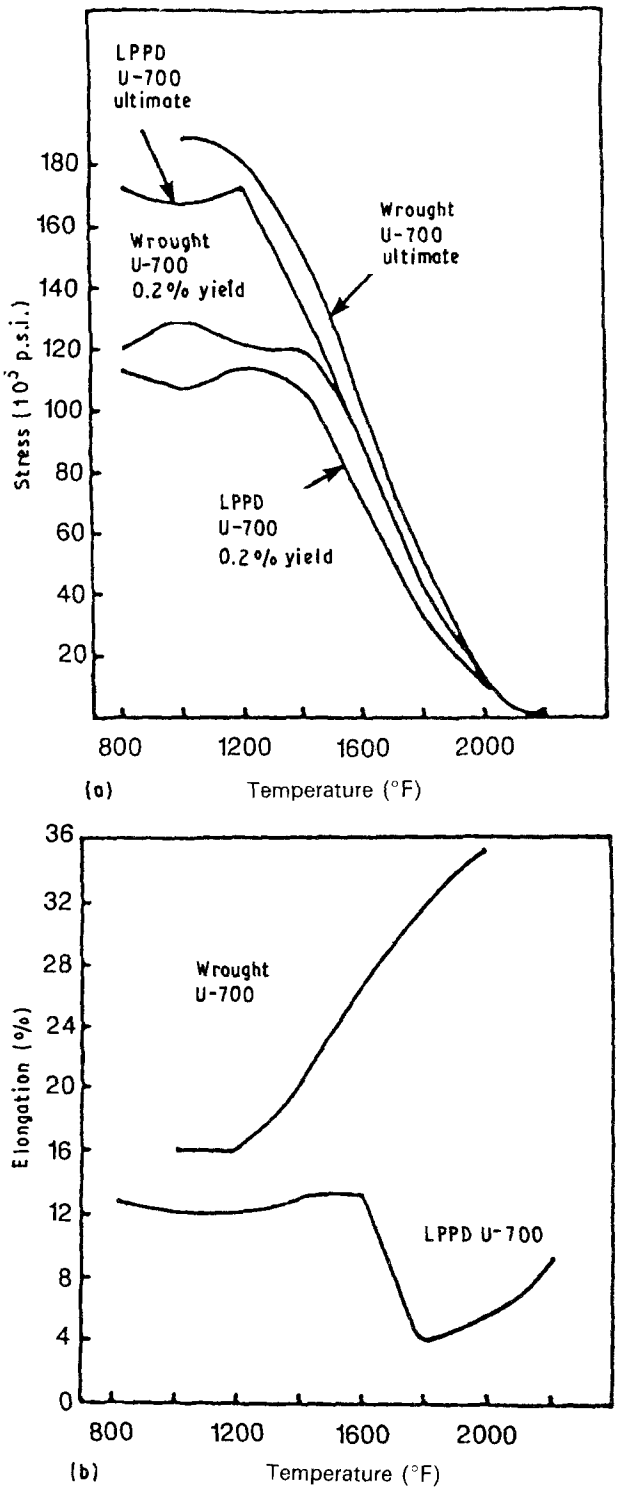

Figure 9 (a) Tensile strengths and (b) ductility as a function of temperature for plasma-deposited (LPPD) and wrought U-700 [38].

the deposits contributed to strength. In a subsequent study, Taub and Jackson [70] highlighted the advantages of plasma-spray forming aluminides and superalloys, the benefit being an ability to produce a rapidly solidified form in the deposited state, without the need for thermomechanical processing.

Two-phase nickel aluminides were produced by vacuum plasma spraying and its microstructure and mechanical properties examined by Sampath *et al.* [37]. The as-sprayed deposit was found to comprise of ordered $L1_2$:Ni_3Al and B2:NiAl phases with an absence of the Ni_5Al_3 compound. The high substrate–deposit temperature achieved during processing

(> 800 °C) followed by fast cooling to room temperature was responsible for the non-formation of Ni_5Al_3 because this phase is thermodynamically unstable at temperatures above 725 °C. Formation of any Ni_5Al_3 from Ni_3Al and NiAl is a slow process and occurs on prolonged exposure to temperature of 700 °C. Annealing the as-sprayed deposit at 1100 °C was found to cause grain coarsening with a concomitant increase in the mean separation distance between the precipitate particles. An increase in annealing time was observed to result in further coarsening in the microstructure. The density and mechanical properties of the as-sprayed and annealed samples, taken from this experimental study, are summarized in Table V [37]. The increase in density with annealing the as-sprayed deposit was attributed to sintering effects. The material revealed essentially brittle fracture at room temperature. However, Sampath *et al.* found the fracture strength of the material to increase from 445 MPa on annealing for 2 h at 1100 °C to 520 MPa on annealing for 24 h at 1100 °C. The as-sprayed sample showed evidence of strain to failure (0.45%), while the annealed counterparts showed considerable degradation in strain to failure. The observed improvement in fracture strength with annealing was rationalized as being due to competing influences of [37]:

(a) an improved interparticle bonding due to sintering, and

(b) a lower number of interphases in the annealed material due to the occurrence of grain growth, thereby reducing the potential regions of failure.

The characteristics of vacuum plasma spray processed nickel aluminide intermetallic alloys: a single-phase Ni_3Al (Cr.Hf.B) and a two-phase NiAl + Ni_3Al, were studied by Sampath *et al.* [34]. In particular, microstructural influences on mechanical properties of the deposits were examined in relation to processing conditions. The deposits produced were found to be thick and dense and had a fine-grained microstructure. Mechanical property results revealed higher strengths for the plasma-sprayed materials compared to the conventionally processed counterparts. However, the VPS materials exhibited poor ductility. Annealing the materials at 1100 °C for 2 h was found to improve ductility and degrade the yield strength and fracture strength of the single-phase Ni_3Al-(Cr.Hf.B) alloy. The degradation in fracture strength was attributed to increasing grain size resulting from annealing. The improvement in ductility was rationalized as being due to improved interparticle bonding of the annealed deposit as compared to the as-sprayed case [34]. In the case of the two-phase alloy, annealing enhanced fracture strength (Table V) and this enhancement was attributed to improved interparticle bonding due to sintering and a reduced number of interfaces due to coarsening. The short exposure to elevated temperatures during VPS processing facilitated interparticle bonding due to diffusion reactions while concurrently aiding relief of the residual stresses associated with deposition, thereby minimizing regions of stress concentration. Thus, the technique of vacuum plasma spraying resulted in homogeneous, stress-free and fine-grained microstructures.

Dense $MoSi_2$ and TiB_2 reinforced $MoSi_2$-based composites were fabricated using the technique of vacuum plasma spraying [36]. The $MoSi_2$ powder had an average particle size of less than 44 μm. The powder stock was then premixed with 20 vol % TiB_2 powder and the resultant mixture was used as feedstock powder for spray forming the composite. These researchers found that approximately 98% theoretical density was obtained by using the technique of vacuum plasma spraying. Subsequent annealing of the spray-formed $MoSi_2$ at 1100 °C was found to lower the density of the deposit. These researchers also found that use of premixed feedstock powder resulted in an injection of the TiB_2 particles into the core of the flame of the plasma gun. The extremely high temperatures at the core of the flame, approximately 10 000 K, caused the TiB_2 particles to melt together with the $MoSi_2$ powder. The resultant hardness of the spray-formed $MoSi_2$ was high, and was attributed to the fine grain size resulting from the VPS process. Annealing the spray-formed deposit for prolonged periods lead to a decrease in hardness and an improvement in fracture toughness. The use of TiB_2 reinforcement in the $MoSi_2$ matrix was found by Tiwari *et al.* to lower the hardness and cause a substantial improvement in toughness of the spray-formed product [36]. The increase in toughness of the spray-formed $MoSi_2$ composite was attributed to the plausible mechanism of arrest of crack propagation.

Tiwari and Herman [71] also developed a theoretical rationale for the incorporation of reinforcements during high-velocity spray forming of metal-matrix composites. The kinetic energy of a rigid particulate on impacting a surface is stored as elastic and plastic strain energy in the surface. Assuming the elastic strain energy to be a very small fraction of the plastic strain energy, the bulk of the energy of the impinging particle is used up in the formation of a small crater on the impinged surface. The average elastic pressure, P_{av}, exerted on the substrate surface by the impacting

TABLE V Room-temperature mechanical properties of the VPS processed and annealed samples of NiAl–Ni_3Al alloy [37]

Material condition	Density (g cm^{-3})	Fracture strength (MPa)	Strain to fracture (%)
As-sprayed	6.29	375	0.45
1100 °C/2 h	6.36	445	0.22
1100 °C/24 h	6.41	520	0.20
Extruded Ni-34 at % Al [68]	–	350	0

particles was initially provided by Hertz [72] and is

$$P_{av} = 0.558\left\{\rho\left[1\Big/\left(\frac{1-\nu_1^2}{E_1}+\frac{1-\nu_2^2}{E_2}\right)\right]^4\right\}^{0.2} V^{0.4} \quad (3)$$

where ρ is the density of the impinging particle, ν is Poisson's ratio, E is Young's modulus, the subscripts 1 and 2 refer to the metallic substrate and the impinging particle, and V is the velocity of the impinging particle. Assuming $E_1 <<< E_2$, then

$$P_{av} = 0.558\left[\rho\left(\frac{E_1}{1-\nu_1^2}\right)^4\right]^{0.2} V^{0.4} \quad (4)$$

For the impinging particle to form a crater on the substrate or impinged surface, the pressure exerted must exceed the yield strength of the substrate material. The pressure exerted on the substrate surface is compared with matrix yield strength of the substrate at the impinging temperature to determine if deformation of the matrix does occur during impact. Tiwari and Herman [71] extended and applied the model for matrices of 308L steel and aluminium alloy 2319. The elastic pressure exerted by an impinging alumina particle was found to be 45 GPa on 308L steel and only 19 GPa on aluminium alloy 2319. These values were found to be greater than the yield strength of the respective matrix alloys at 300 °C (172 MPa for 308L stainless steel and 55 MPa for aluminium alloy 2319). Consequently, plastic deformation is favoured and the impinging particle forms a crater on the substrate surface. Knowing the average size of the alumina particles and their velocity, the kinetic energy of the impinging particle is known. Using Rickerby and Macmillan's [73] equation for depth of crater caused by an impinging particle, Tiwari and Herman [71] found that for successful incorporation of reinforcements in the matrix, during high-velocity spray forming, the depth of penetration must be at least equal in magnitude to the size (dimension) of the reinforcing particle. The depth of penetration being dependent upon the mechanical properties of the matrix alloy at the temperature of deposition. The extent of incorporation of reinforcement into the matrix alloy was found to be dependent upon: (a) the depth of the reinforcement, which should be of similar magnitude as dimensions of the reinforcement, and (b) the nature of matrix-particle bonding. A strong matrix–particle bonding was responsible for mechanical locking of the alumina particle reinforcements in the crater formed during spray forming. Poor bonding between the matrix and the reinforcing particle promotes rebounding of reinforcements resulting in no incorporation of the reinforcement particle (alumina) in the metal matrix.

4. Modified gas welding techniques

In this technique the gas metal arc (GMA) welding torch is modified, wherein aluminium or aluminium alloy wire feed stock is melted and combined with silicon carbide particulates (SiC_p) or silicon carbide whiskers (SiC_w) entrained in an inert gas. Upon striking a substrate or mould, the mixture of aluminium and SiC solidifies into a composite structure [38]. A schematic illustration of the deposition process is shown in Fig. 10.

An arc between the end of the aluminium wire and a water-cooled copper cathode produces a stream of droplets of about 1 mm diameter. At about 230 A the melting rates are on the order of 2 kg h^{-1}. The thermal history of these droplets is controlled to some extent by [38]:

(a) the electrical parameters of the melting process,
(b) the shielding gas used, and
(c) the distance from the orifice to the mould or substrate.

Thermal control of the solidification is also affected by the thermal properties of the mould or substrate. At any instant in time, very little liquid is present, but adequate to bond successive droplets and any SiC reinforcement present. In this technique, the reinforcement material is not substantially affected by fluid flow and solidification macrosegregation. Using appropriate moulds and substrates, complex parts and near-net shapes of the composite structure can be made. The process could be developed into a welding technique for metal-matrix composites that would provide weld metal of approximately the same composition as the base material, thereby reducing the need for mechanical fasteners and adhesives in the fabrication of large structures.

The advantages of this technique are manifold and include [38]

1. an ability to melt, by the arc, any metal, including very high temperature alloys;
2. an ability to entrain any reinforcement in the shielding gas, thus providing a wide variety of reinforced metallic matrices or composite materials;

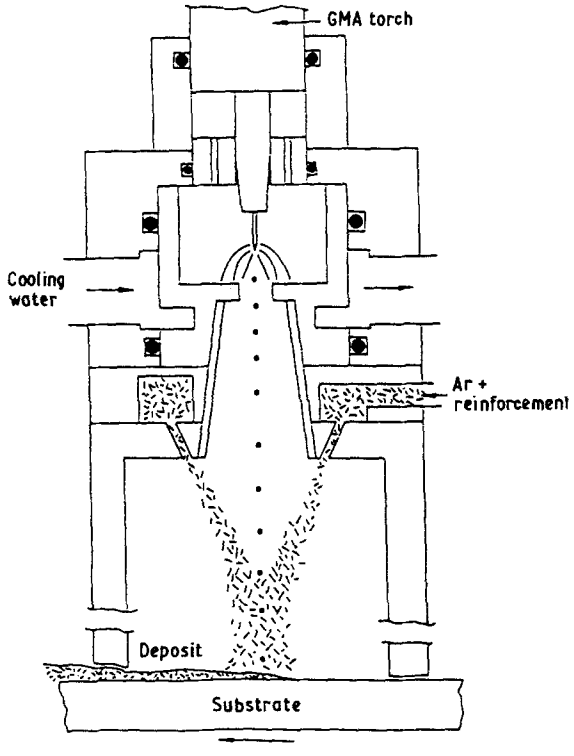

Figure 10 Schematic drawing of modified gas metal arc welding deposition process [38].

3. melting is more convenient than conventional melting methods, because it can be turned on and off at ease,

4. an ability to produce large droplets, thereby minimizing explosion hazards associated with finely divided aluminium powder, and

5. the modified gas metal arc torch is compact, inexpensive and controllable.

The microstructure of an unreinforced material produced by the spray casting process is shown in Fig. 11. The microstructures of metal-matrix composites produced by the modified gas welding technique are shown in Fig. 12. The distribution of reinforcement particles in the MMCs was seen to be uneven, comprising of regions having desirable volume fractions of particles (Fig. 12a) and desirable arrangement of whiskers (Fig. 12b), and also regions in the matrix with little or no silicon carbide. Regions in the matrix containing excessive volume fractions of SiC were not observed. Depending on the coating condition in the mould or substrate, the grain size of the deposits varied or ranged from 42–66 μm [38].

Overall, the modified gas welding technique is stable and can be operated for several minutes, with controllable termination as the end of the substrate is approached. The potential problems associated with the operation of this process include:

(a) clogging of the orifice,

(b) arc instabilities, and

(c) arc extinction due to gas flow imbalances.

However, for the process to be successful, proper shielding of the droplet stream and solidifying metal are both important and essential, in order to produce a good surface finish while keeping internal porosity at a low level. With a high-quality matrix coupled with the ability to add variable amounts and kinds of reinforcements, this technique facilitated microstructural control of metal-matrix composites.

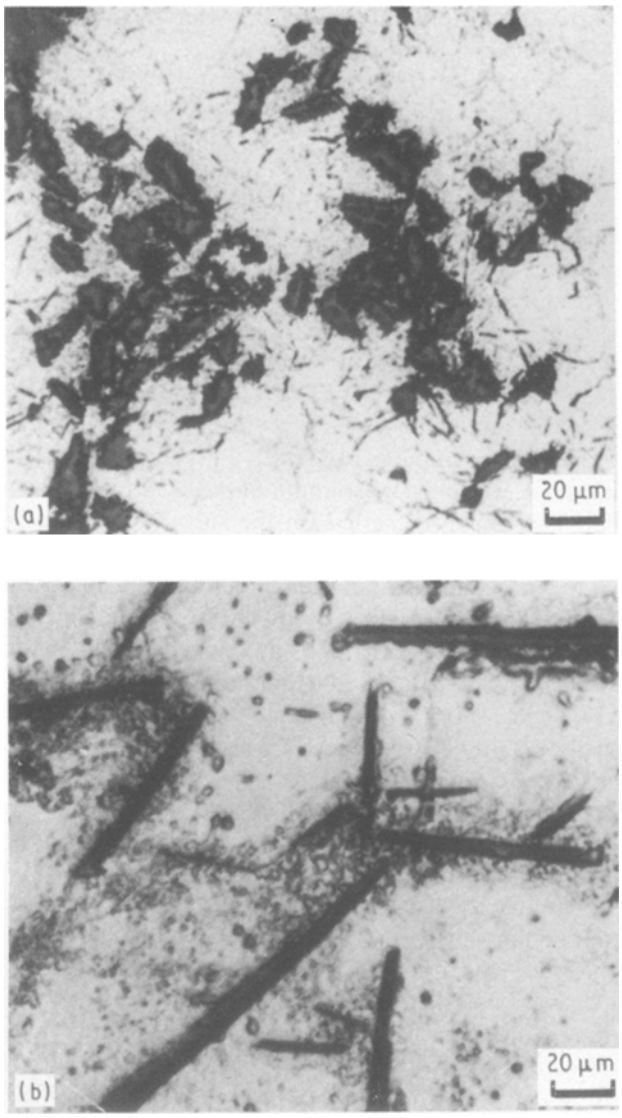

Figure 12 (a) Micrograph showing silicon carbide particulates in a matrix of 1100 aluminium [38]. (b) Micrograph showing silicon carbide whiskers in a matrix of 1100 aluminium [38].

5. High-velocity oxyfuel spraying

High-velocity oxyfuel (HVOF) thermal spraying is the most significant development in the thermal-spray industry since the development of plasma spraying. The rapid growth of this technology can be attributed, to a large degree, to an extensive development of materials and equipment following the introduction of the Jet Kote HVOF spray process in 1982 [39]. Early years saw the technique being used exclusively for aircraft/aerospace applications and part reconditioning. However, with time, the applications of HVOF have expanded from the initial use of tungsten carbide coatings to include hundreds of different coatings that provide for wear, erosion/corrosion resistance, restoration and clearance control of components [39]. A wide variety of coating materials can be sprayed using high-velocity oxyfuel thermal spray technique. However, the process has been used more for the application of carbides.

The HVOF thermal spraying process uses an internal combustion (rocket) jet to generate hypersonic gas velocities of 1830 m s^{-1} (6000 ft s^{-1}), more than five times the speed of sound. Some of the combustion fuels used included propylene, acetylene, propane and hydrogen gases for spraying both carbide and

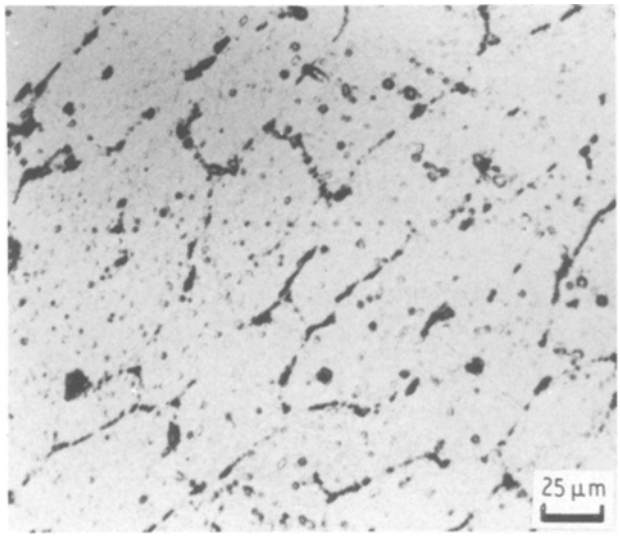

Figure 11 Typical microstructure of 1100 aluminium produced by the spray-casting process [38].

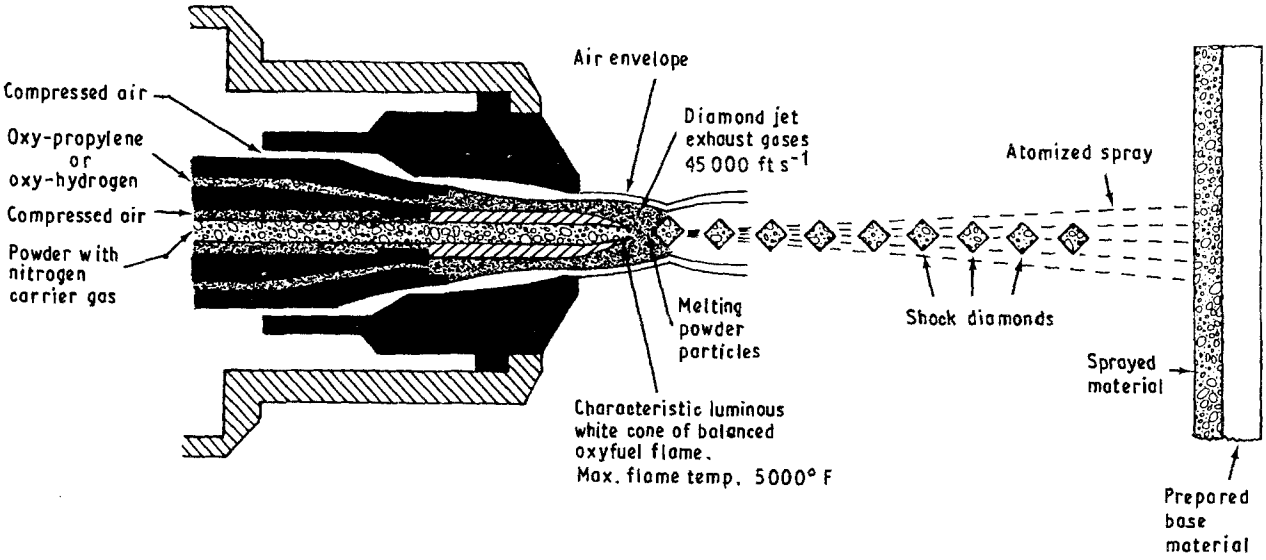

Figure 13 Schematic drawing showing a cross-section of the high-velocity oxyfuel gun [39].

non-carbide coating materials. When burned in an atmosphere or in conjunction with pure oxygen, these fuels produce gas temperatures greater than 2760 °C (5000 °F). A schematic drawing of the high-velocity oxyfuel gun is shown in Fig. 13.

The combustion ignition, gas control and power feed are fundamentally simple in the HVOF spraying system. A pilot flame, typically operating on hydrogen and oxygen is ignited manually, and flow rates of two main jet gases are controlled by a flow meter. Electrically operated solenoids activate the main combustion jet. The flow of powder is electrically controlled and feed rates are monitored automatically. Powders deposited using the HVOF thermal spraying include pure metals, metal alloys, carbides, certain ceramics and even plastics. In fact, early use of the HVOF thermal spraying technology was for carbide coatings on aircraft gas turbine engine components, which experienced wear from abrasion, adhesion, erosion, fretting and corrosion. The key parameters influencing wear resistance of carbide coatings are flame temperature and particle velocity. An additional advantage of this spraying technique is that the tungsten carbide coatings produced are better than those obtained using plasma systems in terms of higher hardness, higher coating bond strength, lower oxide content and porosity, improved wear resistance combined with low residual stress in the coating. Furthermore, the microstructures resulting from HVOF spraying are equal, or better than, those of the highest quality plasma-sprayed coatings. The HVOF coatings show no cracking, spalling or delamination after heating to temperatures as high as 1095 °C (2000 °F) in air and quenching in liquid freon. The HVOF thermal spraying of coatings is shown in Fig. 14.

Several independent tests have shown that the bond strength, while meeting the specification minimum at a coating thickness of 0.25 mm (0.01 in) decreases with an increase in coating thickness to about 39 MPa at 1.5 mm [39]. The same study also showed that bond strength, along with other properties, does not degrade with increasing spray angle (up to 45° from

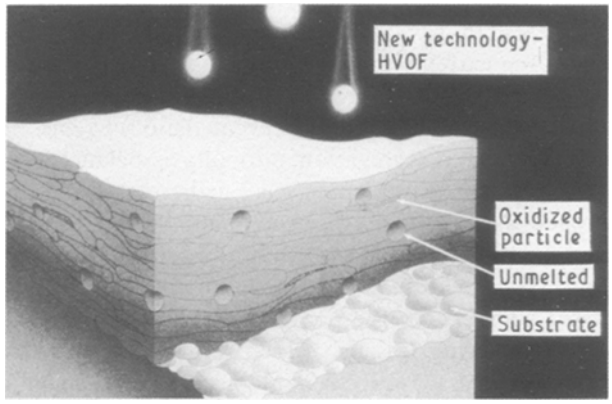

Figure 14 Micrograph showing HVOF thermal spraying propelling coating powders on to the substrate at very high velocities, which flattens the particles creating a higher density coating than is possible using other spraying processes [39].

perpendicular) as had been expected. For example, the bond strength of 0.25 mm thick coatings decreased from about 70 MPa (10^4 p.s.i.) at a spray angle of 0°, to 58 MPa (8.5×10^3 p.s.i.) at a spray angle of 22.5° and to 56.5 MPa (8.2×10^3 p.s.i.) for a spray angle of 45°. However, both macroscopic and microscopic hardness remained unchanged with changes in spray angle.

The most significant and noteworthy advantages of the HVOF process over conventional plasma spraying are higher coating bond strength, lower oxide content and improved wear resistance (predicted based on the higher hardness of the HVOF-sprayed coating). HVOF spraying also has a deposit efficiency of 75% compared with 45% for plasma spraying (Table VI). Besides, HVOF spraying has only one-half as many spraying parameters to control compared with plasma spraying; thus, the process is simpler, enhancing coating reproducibility [39].

6. Conclusion

The development of spray processes for the manufacture of particulate-reinforced metal-matrix composites

TABLE VI Spray-system characteristics for copper–nickel–indium coating [39]

	Spray system	
	HVOF	Plasma
Lap-shear bond strength (p.s.i.)	7300	6200
Tensile bond strength (p.s.i.)	5200	4400
Microstructure		
Oxide content (%)	12	23
Porosity (%)	< 0.5	< 0.5
Hardness		
Macro HR15T	89	83
Micro DPH300	230	160
Deposit efficiency (%)	75	45

was motivated by the difficulties associated with the currently available casting and powder metallurgical processes. In principle, such an approach will help avoid the extreme thermal excursions, and concomitant degradation in interfacial properties. The spray-processing techniques also prevent the occurrence of extensive macrosegregation, normally associated with conventional casting processes. Furthermore, this approach also eliminates the need to handle fine reactive particulates, as is necessary with powder metallurgical processes. The results presented and discussed in this paper suggest that the preliminary findings obtained are encouraging. It is also evident, however, that it will be both necessary and essential to develop an in-depth understanding of the fundamental physical phenomenon involved before such a process can measure up to its commercial potential. The latter will be a challenging task for the scientific community, in view of the complex fluid, thermal and solidification phenomena involved.

Acknowledgements

E. J. L. is very grateful to the Office of Naval Research (Grant N00014-90-J-1923), and the National Science Foundation (Grant MSS 8957449) for their financial support and encouragement. In addition, the author expresses his gratitude to his graduate students, staff and colleagues for numerous stimulating discussions. T. S. S acknowledges with thanks the State of Ohio, Board of Regents (Grants 5-34021 and 5-34126) and ALCOA Foundation (Grant 540341:843) for their support.

References

1. S. G. FISHMAN, *J. Metals* **38**(3) (1986) 26.
2. Y. FLOM and R. J. ARSENAULT, *Mater. Sci. Engng* **77** (1986) 191.
3. T. W. CHOU, A. KELLY and A. OKURA, *Composites* **16** (1985) 187.
4. L. N. MUELLER, J. L. PROHASKA and J. W. DAVIS, in "Proceedings of AIAA Aerospace Engineering Conference" (AIAA, Los Angeles, CA, 1985).
5. A. P. DIVECHA, S. G. FISHMAN and S. D. KARMARKAR, *J. Metals* **33**(9) (1981) 12.
6. R. J. ARSENAULT, *Mater. Sci. Engng* **64** (1984) 171.
7. C. R. CROWE, R. A. GRAY and D. F. HASSON, in "Proceedings of 5th International Conference on Composite Materials", edited by W. C. Harrigan Jr, J. Strife and A. K. Dhingra (The Metallurgical Society of AIME, Warrendale, PA, 1985) p. 843.
8. S. V. NAIR, J. K. TIEN and R. C. BATES, *Int. Metals Rev.* **30** (1985) 275.
9. I. A. IBRAHIM, F. A. MOHAMED and E. J. LAVERNIA, *J. Mater. Sci.* **26** (1991) 1137.
10. C. R. CROWE and D. F. HASSON, in "Proceedings of the Sixth International Conference", edited by R. C. Gifkins (Pergamon Press, Australia, 1982).
11. H. J. RACK, *Adv. Mater. Manufact. Process.* **3**(3) (1988) 327.
12. T. S. SRIVATSAN, I. A. IBRAHIM, F. A. MOHAMED and E. J. LAVERNIA, *J. Mater. Sci.* **27** (1992) 5965.
13. D. L. DAVIDSON, *Metall. Trans.* **18A** (1987) 2125.
14. D. L. McDANELS, *ibid.* **16A** (1985) 1105.
15. W. A. LOGSDON and P. K. LIAW, *Engng Fract. Mech.* **24** (1986) 737.
16. S. MANOHARAN and J. J. LEWANDOWSKI, *Acta Metall.* **38** (1990) 489.
17. D. L. DAVIDSON, *Engng Fract. Mech.* **33** (1989) 965.
18. *Idem, Metall. Trans.* **22A** (1991) 97.
19. JIAN KU SHANG and R. O. RITCHIE, *ibid.* **20A** (1989) 897.
20. M. GUPTA, F. A. MOHAMED and E. J. LAVERNIA, *Mater. Manufact. Process.* **5**(2) (1990) 165.
21. *Idem, Int. J. Rapid Solid.* **8** (1992) in press.
22. S. ANNAVARAPU, D. APELIAN and A. LAWLEY, *Metall. Trans.* **19A** (1988) 3077.
23. R. H. BRICKNELL, *ibid.* **17A** (1986) 583.
24. J. ZHANG, M. N. GUNGOR and E. J. LAVERNIA, in "Conference Proceedings of Eighth International Conference on Composite Materials", ICCM-8, edited by S. W. Tsai and G. S. Springer (SAMPE, Covina, CA, 1991) pp. 17-H-1 to 17-H-12.
25. L. Z. ZHUANG, I. MAJEWSKA-GLABUS, R. VETTER and J. DUSZCYK, *Scripta Metall.* **24** (1990) 2025.
26. K. A. KOJIMA, R. E. LEWIS and M. J. KAUFMAN, in "Aluminum Lithium Alloys V", edited by T. H. Sanders Jr and E. A. Starke Jr (Materials and Component Engineering Publications, Birmingham, UK, 1989) p. 85.
27. E. J. LAVERNIA, *Int. J. Rapid Solid.* **5** (1989) 47.
28. T. C. WILLIS, *Metals Mater.* **4** (1988) 485.
29. A. R. E. SINGER and S. OZBEK, *Powder Metall.* **28**(2) (1985) 72.
30. P. S. GRANT, W. T. KIM, B. P. BEWLAY and B. CANTOR, *Scripta Metall.* **23** (1989) 1651.
31. A. L. MORAN and W. A. PALKO, *J. Metals* **40**(12) (1988) p. 12.
32. E. GUTIERREZ, E. J. LAVERNIA, G. TRAPAGA, J. SZEKELY and N. J. GRANT, *Metall. Trans.* **20A** (1989) 71.
33. D. APELIAN, D. WEI and B. FAROUK, *ibid.* **20B** (1989) 251.
34. S. SAMPATH, B. GUDMUNDSSON, R. TIWARI and H. HERMAN, in "Proceedings Third National Thermay Spray Conference", Cincinnati, October 1988 (ASM International, Metals Park, OH, 1988).
35. R. TIWARI, H. HERMAN, S. SAMPATH and B. GUDMUNDSSON, in 'Proceedings of the Symposium on "Innovative Inorganic Composites"', edited by S. G. Fishman (TMS, Warrendale, PA, 1991).
36. R. TIWARI, H. HERMAN and S. SAMPATH, presented at Materials Research Society, 1990 Fall Meeting.
37. S. SAMPATH, R. TIWARI, B. GUDMUNDSSON and H. HERMAN, *Scripta Metall.* **25** (1991) 1425.
38. C. L. BUHRMASTER, D. E. CLARK and H. B. SMARTT, *J. Metals* November **40** (1988) 44.
39. D. W. PARKER and G. L. KUTNER, *Adv. Mater. Process.* **140** April (1991) 68.
40. Y. WU and E. J. LAVERNIA, *J. Metals* **43**(8) (1991) 16.
41. D. R. UHLMANN, B. CHALMERS and K. A. JACKSON, *J. Appl. Phys.* **35** (1964) 2986.

42. G. F. BOLLING and J. CISSE, *J. Crystal Growth* **10** (1971) 56.
43. T. ERTUK, J. A. CORNIE and R. G. DIXON, in "Interfaces in Metal Matrix Composites", edited by A. K. Dhingra and S. G. Fishman, Conference Proceedings (TMS, Warrendale, PA, 1986) p. 239.
44. A. M. ZUBKO, V. G. LOBANOV and V. V. NIKONOVA, *Sov. Phys. Crystallogr.* **18** (1973) 239.
45. R. MEHRABIAN, R. G. RIEK and M. C. FLEMINGS, *Metall. Trans.* **5A** (1974) 1899.
46. M. K. SURAPPA and P. K. ROHATGI, *J. Mater. Sci. Lett.* **16** (1981) 765.
47. D. M. STEFANESCU, B. K. DHINDAW, S. A. KACAR and A. MOITRA, *Metall. Trans.* **19A** (1988) 2847.
48. P. K. ROHATGI, R. ASTHANA and S. DAS, *Int. Metals Rev.* **31**(3) (1988) p. 115.
49. I. A. IBRAHIM, F. A. MOHAMED and E. J. LAVERNIA, in "Advanced Aluminum and Magnesium Alloys", edited by T. Khan and G. Effenberg (ASM International, Metals Park, OH, 1990) p. 745.
50. I. A. IBRAHIM, E. J. LAVERNIA and F. A. MOHAMED, *J. Mater. Sci.* **26** (1991) 1137.
51. T. S. SRIVATSAN, MANOJ GUPTA, F. A. MOHAMED and E. J. LAVERNIA, *Aluminium* **68** (1992) in press.
52. T. S. SRIVATSAN, RAHUL AURADKAR, AMIT PRAKASH and E. J. LAVERNIA, in "Fracture of Engineering Materials and Structures" (Pergamon Press, Singapore, 1991).
53. T. S. SRIVATSAN and E. J. LAVERNIA, *Compos. Sci. Technol.* (1992) submitted.
54. H. J. RACK and R. W. KRENZER, *Metall. Trans.* **8A** (1977) 35.
55. H. J. RACK, in "Proceedings of the 6th International Conference on Composite Materials", edited by F. L. Mathews, N. C. R. Bushkell, J. M. Hodgkinson and J. Morton (Elsevier Applied Science, London, 1987) p. 2.382.
56. W. A. JOHNSON, "Baseline property and fabrication data for Silicon Carbide Whisker Reinforced Aluminum Alloy", Final Report, Contract N60921-81-C-A238 (1984).
57. H. J. RACK, in "Dispersion Strengthened Aluminum Alloys", edited by Y-M Kim (Metallurgical Society of AIME, Warrendale, PA, 1990) p. 649.
58. H. J. RACK, *Mater. Sci. Engng* **29** (1977) 179.
59. J. E. HATCH (ed.), "Aluminum: Properties and Metallurgy" (ASM, Metals Park, OH, 1984).
60. M. VOGELSANG, R. J. ARSENAULT and R. M. FISHER, *Metall. Trans.* **17A** (1986) 379.
61. R. ARONE, O. BOTSTEIN and B. SHPIGLER, *Israel J. Technol.* **24** (1988) 393.
62. P. NISKANEN and W. R. MOHN, *Adv. Mater. Process.* **3** (1988) 39.
63. J. WHITE, I. G. PALMER, I. R. HUGHES and S. A. COURT, in "Aluminum-Lithium Alloys V", edited by E. A. Starke Jr and T. H. Sanders Jr (Materials and Component Engineering Publication, Birmingham, UK, 1989) p. 1635.
64. T. S. SRIVATSAN, RAHUL AURADKAR, E. J. LAVERNIA and AMIT PRAKASH, *Mater. Trans. JIM* **32** (1991) 473.
65. L. F. COFFIN, *Trans. ASME* **76** (1954) 931.
66. S. S. MANSON, NASA Technical Note, 12954 (NASA, Cleveland, OH) p. 2933.
67. A. SICKINGER and E. MUEHLBERGER, Electroplasma Inc., Irvine CA (1991) current research.
68. P. S. KHADKIKAR, K. VEDULA and B. S. SHABEL, *Mater. Res. Soc. Symp. Proc.* **81** (1987) 157.
69. K. M. CHANG, A. I. TAUB and S. C. HUANG, *ibid.* **39** (1985) 335.
70. A. I. TAUB and M. R. JACKSON, *ibid.* **58** (1986) 389.
71. R. TIWARI and H. HERMAN, *Scripta Metall.* in press.
72. H. HERTZ, *J. Reine Angew Math.* **92** (1891) p. 156.
73. D. G. RICKERBY and N. H. MACMILLAN, in "Proceedings of the 5th International Conference on Erosion by Liquid and Solid Impact", Cambridge, UK (Cambridge University Press, 1979) p. 29.

Received 27 November
and accepted 12 December 1991